Article

Super-Twisting Extended State Observer and Sliding Mode Controller for Quadrotor UAV Attitude System in Presence of Wind Gust and Actuator Faults

Di Shi [1] , **Zhong Wu** [1,*] **and Wusheng Chou** [2,3]

1   School of Instrumentation Science and Optoelectronics Engineering, Beihang University, Beijing 100191, China; shidi666@buaa.edu.cn
2   School of Mechanical Engineering and Automation, Beihang University, Beijing 100191, China; wschou@buaa.edu.cn
3   State Key Laboratory of Virtual Reality Technology and System, Beijing 100191, China
*   Correspondence: wuzhong@buaa.edu.cn; Tel.: +86-10-8233-9703

check for updates

Abstract: This article addresses the problem of high precision attitude control for quadrotor unmanned aerial vehicle in presence of wind gust and actuator faults. We consider the effect of those factors as lumped disturbances, and in order to realize the quickly and accurately estimation of the disturbances, we propose a control strategy based on the online disturbance uncertainty estimation and attenuation method. Firstly, an enhanced extended state observer (ESO) is constructed based on the super-twisting (ST) algorithm to estimate and attenuate the impact of wind gust and actuator faults in finite time. And the convergence analysis and parameter selection rule of STESO are given following. Secondly, in order to guarantee the asymptotic convergence of desired attitude timely, a sliding mode control law is derived based on the super-twisting algorithm. And a comprehensive stability analysis for the entire system is presented based on the Lyapunov stability theory. Finally, to demonstrate the efficiency of the proposed solution, numerical simulations and real time experiments are carried out in presences of wind disturbance and actuator faults.

Keywords: quadrotor; super twisting extended state observer (STESO); super twisting sliding mode controller (STSMC); wind disturbance; actuator faults

1. Introduction

Quadrotor unmanned aerial vehicles (UAVs) are rapidly growing in popularity due to their wide range of civil and military applications such as surveillance, inspection, search and rescue, and disaster response. As a new kind of UAV, quadrotor is a small rotorcraft with four propellers driven by four direct current (DC) motors respectively [1]. Compared with traditional helicopters, the structure of quadrotor is simpler and more efficient, and has unique features in precise hovering, aggressive maneuver, vertical take-off and landing (VTOL) [2,3], etc. Therefore, the researches on quadrotor unmanned aerial vehicle become more and more popular in recent years, and a lot of achievements have been made [4–6].

The quadrotor is an underactuated and nonlinear coupled system [7]. Traditionally, the integral-type control methods are commonly used in the controller design of quadrotor UAVs and have shown to be effective in the attitude and position stabilization control of them. In [8,9], a proportional integral derivative (PID) control method was developed to obtain the stability of quadrotor. In [10], nonlinear PI/PID controller was designed to regulate the posture of quadrotor and showed robustness to aircraft systems effects. In [11], a motion controller of quadrotor has been derived by using time scale separation ideas, and numerical simulations confirmed that the motion

control objective is satisfied with the proposed scheme in presence of the forces saturation of propellers, sensor noise and perturbing forces caused by wind. And in [12], the linear quadratic regulator (LQR) controller was applied to deal with the nominal system of quadrotor obtained by feedback linearization method. In order to meet some mission requirements, high precision attitude control is essential in those applications. However, when operating in outdoor environments, quadrotors would be easily affected by wind gust during the course of flight [13]. In addition to wind gust, the actuating motor-propeller system is prone to faults due to component degradation or damage to the motors or propellers, which may lead to significant performance degradation or even instability of the close-loop system [14]. Therefore, it is difficult for the traditional linear controllers to achieve the high precision control requirement under the influence of these factors. To solve this problem, many approaches have been proposed in literatures. Robust adaptive controller was introduced to eliminate the influence of wind gust in [15]. In [16], robust optimal backstepping control (ROBC) is designed to address the stabilization and trajectory tracking problem of quadrotor in the existence of wind gust. And in [14], a nonlinear robust adaptive fault-tolerant altitude and attitude tracking method was implemented to accommodating actuator faults in quadrotor without the need of a faults diagnosis mechanism. In summery, these methods were designed to improve the robustness of the system.

Alternatively, both wind gust and actuator faults can be considered as lumped disturbances and the online disturbance and uncertainty estimation and attenuation (DUEA) method would be a potential solution to this problem. In recent years, the DUEA methods have been widely studied for some types of real time systems in order to cancel the influence of lumped disturbances at the controller stage [17,18], and the framework of which can be divided into two parts, namely, a disturbance and uncertainty estimator (DUE) and a feedback controller (FC).

In the first part, DUE is designed to estimate the disturbances so that they could be compensated in the feedforward loop. To achieve this aim, a series of observers have been proposed as the DUE so far, such as disturbance observer (DO) [19,20], extended state observer (ESO) [21–24], proportional integral observer (PIO) [25,26] and acceleration based disturbance observer (ABDOB) [27], etc. By the appropriate use of the observer, disturbance rejection performance and robustness of the existing control system could be significantly improved. The extended state observer (ESO), known as the key module of active disturbance rejection control, can estimate both the states of system and the total disturbances with less dependence on model information [28,29]. This method was first proposed by Han in 1990s and the basic idea behind ESO is to view disturbance as an extended state and utilize observer to estimate it [28]. As for the ESO based control structure, the performance of closed-loop system is largely determined by the estimation accuracy of observer. The traditional ESO approaches focus primarily on dealing with slowly changing disturbances. However, it's obvious that the disturbance torque caused by the wind gust and actuator faults happens suddenly, which can not be estimated by traditional ESO thoroughly [30]. Therefore, an enhanced ESO that can quickly estimate the disturbance is necessary in this field. In [31], a higher-order ESO is investigated and the estimation accuracy was improved, however, higher level of the observer order will lead to a higher observer gain which will in return excite the sensor noise and introduce them into the control loop. In [32], a sliding model method was used in disturbance observer to estimate the quadrotor velocities, the external disturbances such as wind and parameter uncertainties, and achieves good results, except for serious chattering. To reduce this problem, super-twisting algorithm have been adopted in design of the observer. In [33], the super-twisting observer (STO) is constructed to reject aperiodic disturbances and input unmatched periodic disturbances with reduced chattering.

In the second part, the FC is designed to guarantee fast convergence of the closed-loop system. Sliding mode control (SMC) has been known as one of the most efficiency controller in fast convergence [34]. In [35], a fixed-time second-order sliding mode control law is designed to guarantee the reaching time, independent of initial conditions. However, the robustness of the SMC is achieved at the cost of a high frequency switching of the control signal, which has a negative effect in the actuator.

To reduce the chattering, a family of continuous sliding mode controllers based on super-twisting algorithm have been developed [36].

Motivated by the above observations and inspired from Ref. [33,36], a high precision attitude control law is developed for quadrotor unmanned aerial vehicle in presence of wind gust and actuator faults. The main contributions of this paper are summarized as follows:

- Propose a STESO to accurately estimate the disturbance torque caused by wind gust and actuator faults in finite time, and give the parameter selection rule of the observer;
- Design a fast convergence attitude control law based on STSMC, and give a comprehensive stability analysis on the entire system.

The remainder of the paper is organized as follows. The mathematical model and control problem is formulated in Section 2. A STESO is designed in Section 3, as well as parament selection rule of the observer is also given in this section. In Section 4, a fast convergence attitude controller is designed based on ST algorithm. Numerical simulation and real time experimental results are presented in Section 5. Finally, we conclude the paper in Section 6.

2. Mathematical Model and Problem Formulation

2.1. Notation

$\|\bullet\|$ denotes the 2-norm of a vector or a matrix. For a given vector $v = [v_1, ..., v_n]^T \in \mathbb{R}^n$, $\|v\| = \sqrt{v^T v}$. For a given matrix $A \in \mathbb{R}^{n \times n}$, $\lambda_{\max}(A)$ and $\lambda_{\min}(A)$ denote the maximal and minimum eigenvalue of the matrix respectively. In addition, the operator $S(\bullet)$ maps a vector $x = [\begin{array}{ccc} x_1 & x_2 & x_3 \end{array}]^T$ to a skew symmetric matrix as:

$$S(x) = \begin{bmatrix} 0 & -x_3 & x_2 \\ x_3 & 0 & -x_1 \\ -x_2 & x_1 & 0 \end{bmatrix}$$

$\text{sgn}(\bullet)$ is the sign function, and for a scalar x:

$$\text{sgn} = \begin{cases} \dfrac{x}{|x|}, & |x| \neq 0 \\ 0, & |x| = 0 \end{cases}$$

For a vector $x = [\begin{array}{ccc} x_1 & x_2 & x_3 \end{array}]^T$ and $r \geq 0$, define:

$$\text{sig}(x)^r = \begin{bmatrix} |x_1|^r \, \text{sgn}(x_1) \\ |x_2|^r \, \text{sgn}(x_2) \\ |x_3|^r \, \text{sgn}(x_3) \end{bmatrix}$$

2.2. Quaternion Operations

In order to avoid the singularity problem of trigonometric functions, unit quaternion $q = [\begin{array}{cc} q_0 & q_v^T \end{array}]^T \in \mathbb{R}^4, \|q\| = 1$ is used to represent rotation [37] of the quadrotor. Following are the operations we used.

The quaternion multiplication is:

$$q_1 \otimes q_2 = \begin{bmatrix} q_{01} q_{02} - q_{v1}^T q_{v2} \\ q_{01} q_{v2} + q_{02} q_{v1} - S(q_{v2}) q_{v1} \end{bmatrix} \tag{1}$$

The relationship between rotation matrix C_A^B and q is calculated as:

$$C_A^B = (q_0^2 - q_v^T q_v)I_3 + 2q_v q_v^T + 2q_0 S(q_v) \tag{2}$$

$$\dot{C}_A^B = -S(\boldsymbol{\omega})C_A^B \tag{3}$$

The derivative of a quaternion is given by the quaternion multiplication of the quaternion q and the angular velocity of the system $\boldsymbol{\omega}$:

$$\dot{q} = \begin{bmatrix} \dot{q}_0 \\ \dot{q}_v \end{bmatrix} = \frac{1}{2} q \otimes \begin{bmatrix} 0 \\ \boldsymbol{\omega} \end{bmatrix} = \frac{1}{2} \begin{bmatrix} -q_v^T \\ S(q_v) + q_0 I_3 \end{bmatrix} \boldsymbol{\omega} \tag{4}$$

The quaternion error q_e is given as the quaternion multiplication of the conjugate of the actual quaternion q and the desired quaternion q_d :

$$q_e = q_d^* \otimes q = \begin{bmatrix} q_0 q_{0d} + q_v{}^T q_{vd} \\ q_{0d} q_v - q_0 q_{vd} + S(q_v) q_{vd} \end{bmatrix} \tag{5}$$

2.3. Kinematics and Dynamics of Quadrotor

In this section, the kinematic and dynamic differential equations of the quadrotor are established. The quadrotor can be considered as a rigid cross frame attached with four rotors, and the center of gravity coincides with the body-fixed frame origin.

The simplified model of the quadrotor is presented in Figure 1, rotors $R1$ and $R3$ rotate counterclockwise and rotors $R2$ and $R4$ rotate clockwise. Each propeller rotates at the angular speed $\Omega_i \in [\Omega_{i,min}, \Omega_{i,max}]$ and produces a force F_i ($i = 1, 2, 3, 4$) along the negative z-direction relative to the body frame [37,38]:

$$F_i = \begin{bmatrix} 0 \\ 0 \\ -k_T \Omega_i^2 \end{bmatrix} \tag{6}$$

where $k_T > 0$ denotes the aerodynamic coefficient which consists formed of the atmospheric density ρ, the radius of the propeller r, and the thrust coefficient c_T. In addition, due to the spinning of the rotors, a reaction torque M_i ($i = 1, 2, 3, 4$) is generated on the quadrotor body by each rotor:

$$M_i = \begin{bmatrix} 0 \\ 0 \\ (-1)^{i+1} k_D \Omega_i^2 \end{bmatrix} \tag{7}$$

where $k_D > 0$ denotes the drag coefficient of the rotor, which depends on the same factors as $k_T > 0$.
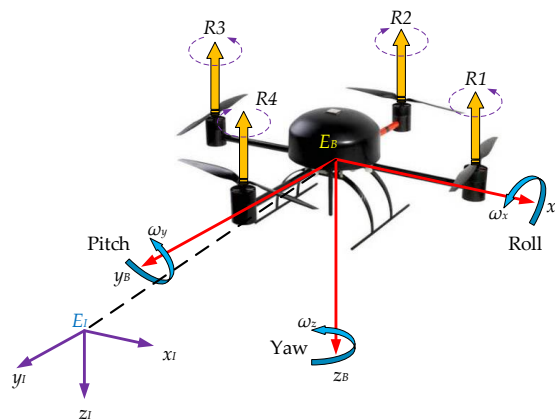

Figure 1. Coordinate systems of the quadrotor.

In the mathematical model of quadrotor, three coordinate frames are considered: the non-moving inertial frame $E_I : \{o_I, x_I, y_I, z_I\}$, the body-fixed frame $E_B : \{o_B, x_B, y_B, z_B\}$ and the desired frame $E_D : \{o_D, x_D, y_D, z_D\}$ to represent the actual attitude and desired attitude of quadrotor respectively. Note that North-East-Down (NED) coordinates are used to define all frames. Attitude angle and angular velocities of the body-fixed frame E_B with respect to the inertial frame E_I are written as $\Theta = \begin{bmatrix} \phi & \theta & \psi \end{bmatrix}^T$ and $\omega = \begin{bmatrix} \omega_x & \omega_y & \omega_z \end{bmatrix}^T$ respectively, and the quaternion expression of the attitude is $q = \begin{bmatrix} q_0 & q_v \end{bmatrix}^T$.

The variation of the orientation is achieved by varying the angular speed of a specific rotor. The torque created around a particular axis with respect to the body-fixed frame is defined as follows:

$$u = \begin{bmatrix} \tau_\phi \\ \tau_\theta \\ \tau_\psi \end{bmatrix} = \overbrace{\begin{bmatrix} 0 & -lk_T & 0 & lk_T \\ lk_T & 0 & -lk_T & 0 \\ -k_D & k_D & -k_D & k_D \end{bmatrix}}^{M} \begin{bmatrix} \Omega_1^2 \\ \Omega_2^2 \\ \Omega_3^2 \\ \Omega_4^2 \end{bmatrix} \tag{8}$$

where l denotes the distance from the rotors to the center of mass and u represents the control signal to be designed.

Assuming a symmetric mass distribution of the quadrotor, the nominal inertia matrix $J = \mathrm{diag}(J_x, J_y, J_z)$ is diagonal. With the disturbances $d = \begin{bmatrix} d_x & d_y & d_z \end{bmatrix}^T$ caused by wind gust d_w and actuator faults d_u into consideration, the attitude dynamic model of the quadrotor can be obtained as the following differential equations:

$$\begin{bmatrix} J_x \dot{\omega}_x \\ J_y \dot{\omega}_y \\ J_z \dot{\omega}_z \end{bmatrix} + \begin{bmatrix} (J_z - J_y)\omega_y\omega_z \\ (J_x - J_z)\omega_x\omega_z \\ (J_y - J_z)\omega_x\omega_y \end{bmatrix} = \begin{bmatrix} \tau_\phi \\ \tau_\theta \\ \tau_\psi \end{bmatrix} + \begin{bmatrix} d_x \\ d_y \\ d_z \end{bmatrix} \tag{9}$$

According to Equation (4), we summarized the mathematical model of the quadrotor as:

$$\begin{cases} \dot{q} = \dfrac{1}{2} q \otimes \begin{bmatrix} 0 & \omega \end{bmatrix}^T \\ \dot{\omega} = -J^{-1}S(\omega)J\omega + J^{-1}u + J^{-1}d \end{cases} \tag{10}$$

In practice, we can use micro electro mechanical system (MEMS) inertial measurement unit (IMU) to measure the attitude information ω and q.

2.4. Lumped Disturbaces

2.4.1. Wind Gust

Wing gust produces a strong disturbance torque on the quadrotor. In this article, a Dryden wind gust model is introduced [39]. We assume that the disturbance caused by wind gust d_w is proportional to the speed of wind gust, therefore, d_w can be described based on the random theory [40] and defined as a summation of sinusoidal excitations:

$$d_{w,k}(t) = d_{w,k}^0 + \sum_{i=1}^{n_k} a_{i,k} \sin(\varpi_{i,k} t + \varphi_{i,k}) \tag{11}$$

where $d_{w,k}(t)$ is a time-dependent description of the wind disturbance in $k = x, y, z$ channel in a given time t. $\varpi_{i,k}$ and $\varphi_{i,k}$ are randomly selected frequencies and phase shifts, $n_{i,k}$ is the number of sinusoids, $a_{i,k}$ is the amplitude of the sinusoid, and $d_{w,k}^0$ is the static wind disturbance.

2.4.2. Actuator Faults

In this article, we consider actuator faults represented by partial loss of effectiveness in the rotors. For instance, caused by structural damage to a propeller [14], battery power loss [41], etc. Thus, the actuator faults in this article are modeled as follows, for $i = 1, ..., 4$:

$$\Omega_i^* = \alpha_i \Omega_i \tag{12}$$

where Ω_i represents the commanded rotor angular velocity, Ω_i^* is the loss of angular velocity, and $\alpha_i \in [0, \bar{\alpha})$ is an unknown ratio characterizing the occurrence of a partial loss of effectiveness fault in rotor i with $\bar{\alpha}$ being a known upper bound needed to maintain the controllability of the quadrotor. For instance, in the extreme case of complete failure $b_i = \bar{\alpha}$, the quadrotor becomes uncontrollable. The case of $b_i = 1$ represents a healthy rotor, and $0 \leq \alpha_i < \bar{\alpha} < 1$ represents a faulty rotor with partial loss of effectiveness.

$$d_u = M \begin{bmatrix} \alpha_1^2 \Omega_1^2 \beta_1 (t - T_1) \\ \alpha_2^2 \Omega_2^2 \beta_2 (t - T_2) \\ \alpha_3^2 \Omega_3^2 \beta_3 (t - T_3) \\ \alpha_4^2 \Omega_4^2 \beta_4 (t - T_4) \end{bmatrix} \tag{13}$$

where the fault time profile function $\beta_i(t - T_i)$ is assumed to be a step function with unknown fault occurrence time T_i for $i = 1, ..., 4$, that is:

$$\beta_i (t - T_i) = \begin{cases} 0, & if \quad t < T_i \\ 1, & if \quad t \geq T_i \end{cases} \tag{14}$$

In summary, we can see that the disturbances $d = d_w + d_u$ acting on quadrotor are high-order, non-Gaussian and happen suddenly, furthermore, their randomness and nonlinearity are also very strong.

2.5. Problem Formulation

The purpose of this article is to achieve the high precision tracking to the desired attitude in presence of wind gust and actuator faults. Therefore, the dynamics of attitude error should be introduced. We use $\omega_d = [\begin{array}{ccc} \omega_{d,x} & \omega_{d,y} & \omega_{d,z} \end{array}]^T$ and $q_d = [\begin{array}{cc} q_{0d} & q_{vd} \end{array}]^T$ to denote the desired angular velocities and attitude respectively, thus the tracking error vector of the angular velocities $\omega_e = [\begin{array}{ccc} \omega_{e,x} & \omega_{e,y} & \omega_{e,z} \end{array}]^T$ can be expressed as:

$$\omega_e = \omega - C_d^b \omega_d \tag{15}$$

Then, we can obtain the dynamics of ω_e according to Equations (3), (10) and (15):

$$\dot{\omega}_e = S(\omega_e) C_d^b \omega_d - C_d^b \dot{\omega}_d - J^{-1} S(\omega) J \omega + J^{-1} u + J^{-1} d \tag{16}$$

where C_d^b can be calculated according to Equations (2) and (5). And according to Equations (4), (5), and (15), we can obtain the kinematics of attitude tracking error:

$$\dot{q}_e = \frac{1}{2} q_e \otimes [\begin{array}{cc} 0 & \omega_e \end{array}]^T = \frac{1}{2} \begin{bmatrix} -q_{ve}^T \\ S(q_{ve}) + q_{0e} I_3 \end{bmatrix} \omega_e \tag{17}$$

Therefore, the problem we try to tackle in this work is to design a continuous control law u, which guarantees errors of attitude angles q_e and angular velocities ω_e asymptotic converge to zero in the presence of the lumped disturbances d.

Figure 2 illustrates the control structure that we designed. Based on the DUEA control methodology, the attitude tracking problem for quadrotor can be divided into two components:

- Design the feedforward loop so that the lumped disturbances are estimated by STESO and compensated this way.
- Design the feedback loop that regulates the orientation of quadrotor to track the desired attitude produced by the commander timely.
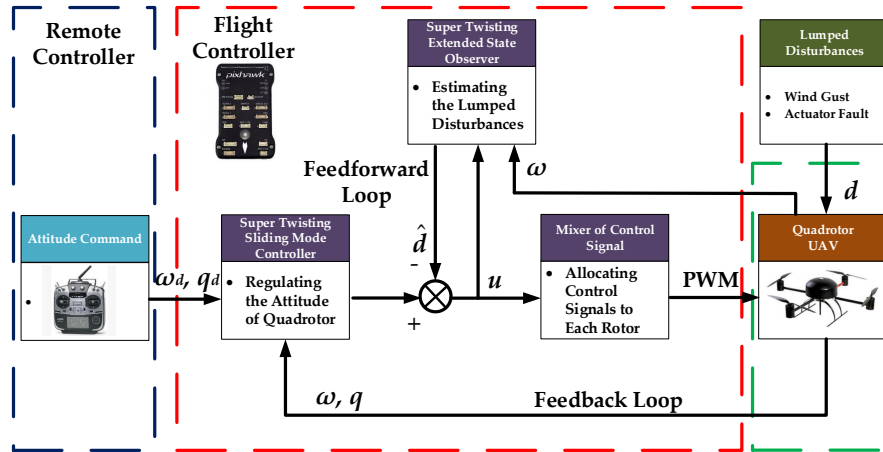

Figure 2. Block diagram of the proposed control scheme.

3. Design and Analysis of Super Twisting Extended State Observer

Through the analysis in previous section, we can see that the lumped disturbances acting on quadrotor are high-order and rapidly changing, therefore, it is difficult for traditional ESO to estimate them thoroughly [30]. Higher-order ESO have been applied in some articles. However, higher observer orders will lead to higher control gains with fixed bandwidth. Which will in return excite the sensor noise and introduce them into the control loop. By introducing super twisting algorithm, excessively high observer gain can be avoided. In this section, the STESO is proposed and the convergence analysis and parameter selection rule of STESO are given.

3.1. Design of STESO

Consider the dynamics Equation (10) of quadrotor, since the angular velocities ω can be measured by the MEMS gyroscope, the original control input can be reformulated by employing the feedback linearization technique as:

$$u = u^* + S(\omega)J\omega \tag{18}$$

Therefore, we can obtain the linearized model of the quadrotor as $J\dot{\omega} = u^* + d$.

It is supposed that each component of the linearized model is independent from each other. Hence, the controller policy developed from one channel can be directly applied to the other two and the description of only the i-th channel is sufficient ($i = x, y, z$). In this way, the one-dimensional dynamic of the quadrotor is obtained as:

$$J_i\dot{\omega}_i = \tau_i^* + d_i \tag{19}$$

Introducing a new state vector $\boldsymbol{\xi_i} = \begin{bmatrix} \xi_{1,i} & \xi_{2,i} \end{bmatrix}^T$ whose components are defined as $\xi_{1,i} = J_i\omega_i$ and augmenting lumped disturbances d_i as an extended state $\xi_{2,i} = d_i$, the reconstructed system is rewritten as:

$$\begin{cases} \dot{\xi}_{1,i} = \xi_{2,i} + \tau_i^* \\ \dot{\xi}_{2,i} = \delta_i \end{cases} \tag{20}$$

where δ_i is the derivative of d_i. Assume that the system states are bounded, then the existence of a constant f_i^+ is ensured such that the inequality $|\delta_i| < f_i^+$ holds for any time.

It can be verify that the pair (A, C) is observable. Then, consider $\hat{\xi}_i$ as the estimation of ξ_i, STESO can be designed as follows:

$$\begin{cases} \dot{\hat{\xi}}_{1,i} = \hat{\xi}_{2,i} + \tau_i^* + a_i \left| \xi_{1,i} - \hat{\xi}_{1,i} \right|^{\frac{1}{2}} \text{sgn} \left(\xi_{1,i} - \hat{\xi}_{1,i} \right) \\ \dot{\hat{\xi}}_{2,i} = b_i \, \text{sgn} \left(\xi_{1,i} - \hat{\xi}_{1,i} \right) \end{cases} \tag{21}$$

where a_i and b_i are the observer gains to be designed.

Define the estimation error variables $\tilde{\boldsymbol{\xi}}_i = \begin{bmatrix} \tilde{\xi}_{1,i} & \tilde{\xi}_{2,i} \end{bmatrix}^T$ as $\tilde{\boldsymbol{\xi}}_i = \boldsymbol{\xi}_i - \hat{\boldsymbol{\xi}}_i$, and the dynamics of the $\tilde{\boldsymbol{\xi}}_i$ can be obtained as follows:

$$\begin{cases} \dot{\tilde{\xi}}_{1,i} = \hat{\xi}_{2,i} - a_i \left| \xi_{1,i} - \hat{\xi}_{1,i} \right|^{\frac{1}{2}} \text{sgn} \left(\xi_{1,i} - \hat{\xi}_{1,i} \right) \\ \dot{\tilde{\xi}}_{2,i} = \delta_i - b_i \, \text{sgn} \left(\xi_{1,i} - \hat{\xi}_{1,i} \right) \end{cases} \tag{22}$$

The dynamics of the estimation error, presented in Equation (22), have the form of a non-recursive exact robust differentiator. Therefore, the errors $\tilde{\xi}_{1,i}$ and $\tilde{\xi}_{2,i}$ will converge to zero in a finite time if the gains a_i and b_i are chosen appropriately. The convergence analysis and parameter selection rule will be demonstrated following.

3.2. Convergence Analysis and Parameter Selection Rule

Firstly, introduce a new state vector $\boldsymbol{\eta}_i = \begin{bmatrix} \eta_{1,i} & \eta_{2,i} \end{bmatrix}^T$ as $\eta_{1,i} = \left| \tilde{\xi}_{1,i} \right|^{\frac{1}{2}} \text{sgn} \left(\tilde{\xi}_{1,i} \right)$, $\eta_{2,i} = \tilde{\xi}_{2,i}$ and take the time derivative of $\boldsymbol{\eta}_i$, we have:

$$\begin{cases} \dot{\eta}_{1,i} = \frac{1}{2} \left| \tilde{\xi}_{1,i} \right|^{-\frac{1}{2}} \left(-a_i \left| \tilde{\xi}_{1,i} \right|^{\frac{1}{2}} \text{sgn} \left(\tilde{\xi}_{1,i} \right) + \tilde{\xi}_{2,i} \right) \\ \dot{\eta}_{2,i} = -b_i \, \text{sgn} \left(\tilde{\xi}_{1,i} \right) + \delta_i \end{cases} \tag{23}$$

which can be rewritten as:

$$\dot{\boldsymbol{\eta}}_i = \left| \tilde{\xi}_{1,i} \right|^{-\frac{1}{2}} \overbrace{\begin{bmatrix} \frac{-a_i}{2} & \frac{1}{2} \\ -b_i & 0 \end{bmatrix}}^{A} \boldsymbol{\eta}_i + \overbrace{\begin{bmatrix} 0 \\ 1 \end{bmatrix}}^{B} \delta_i \tag{24}$$

Then, introduce a positive definite matrix $\boldsymbol{P} = \frac{1}{2} \begin{bmatrix} 4b_i + a_i^2 & -a_i \\ -a_i & 2 \end{bmatrix}$ and consider the following Lyapunov function:

$$V_i = \boldsymbol{\eta}_i^T \boldsymbol{P} \boldsymbol{\eta}_i \tag{25}$$

Notice that in Equation (25), V_i is continuous but is not differentiable at $\tilde{\xi}_{1,i} = 0$, and it is positive definite and radially unbounded if $b_i > 0$, thus we have:

$$\lambda_{\min} (\boldsymbol{P}) \left\| \boldsymbol{\eta}_i \right\|^2 \leq V_i \leq \lambda_{\max} (\boldsymbol{P}) \left\| \boldsymbol{\eta}_i \right\|^2 \tag{26}$$

Take the time derivative of V_i and define $\boldsymbol{Q} = \boldsymbol{A}^T \boldsymbol{P} + \boldsymbol{P} \boldsymbol{A}$, we have:

$$\begin{aligned} \dot{V}_i &= \left| \tilde{\xi}_{1,i} \right|^{-\frac{1}{2}} \boldsymbol{\eta}_i^T \left(\boldsymbol{A}^T \boldsymbol{P} + \boldsymbol{P} \boldsymbol{A} \right) \boldsymbol{\eta}_i + \delta_i \left(\boldsymbol{B}^T \boldsymbol{P} \boldsymbol{\eta}_i + \boldsymbol{\eta}_i^T \boldsymbol{P} \boldsymbol{B} \right) \\ &\leq - \left| \tilde{\xi}_{1,i} \right|^{-\frac{1}{2}} \boldsymbol{\eta}_i^T \boldsymbol{Q} \boldsymbol{\eta}_i + 2 f_i^+ \boldsymbol{B}^T \boldsymbol{P} \boldsymbol{\eta}_i \end{aligned} \tag{27}$$

where $|\delta_i| < f_i^+$ and $\boldsymbol{Q} = \frac{a_i}{2} \begin{bmatrix} 2b_i + a_i^2 & -a_i \\ -a_i & 1 \end{bmatrix}$ is positive defined. Notice that:

$$
\begin{aligned}
2f_i^+ \boldsymbol{B}^T \boldsymbol{P} \boldsymbol{\eta}_i \;&=\; \left|\tilde{\xi}_{1,i}\right|^{-\frac{1}{2}} f_i^+ \left(\left|\tilde{\xi}_{1,i}\right|^{\frac{1}{2}} \left(-a_i \eta_{1,i} + 2\eta_{2,i} \right) \right) \\
&=\; \left|\tilde{\xi}_{1,i}\right|^{-\frac{1}{2}} f_i^+ \left(|\eta_{1,i}| \left(-a_i \eta_{1,i} + 2\eta_{2,i} \right) \right) \\
&\leq\; \left|\tilde{\xi}_{1,i}\right|^{-\frac{1}{2}} f_i^+ \left(a_i |\eta_{1,i}|^2 + 2\,|\eta_{1,i}|\,|\eta_{2,i}| \right) \\
&\leq\; \left|\tilde{\xi}_{1,i}\right|^{-\frac{1}{2}} f_i^+ \left(a_i |\eta_{1,i}|^2 + |\eta_{1,i}|^2 + |\eta_{2,i}|^2 \right) \\
&=\; \left|\tilde{\xi}_{1,i}\right|^{-\frac{1}{2}} \boldsymbol{\eta}_i^T
\begin{bmatrix} f_i^+ (a_i + 1) & 0 \\ 0 & f_i^+ \end{bmatrix}
\boldsymbol{\eta}_i \\
&=\; -\left|\tilde{\xi}_{1,i}\right|^{-\frac{1}{2}} \boldsymbol{\eta}_i^T \Delta \boldsymbol{Q} \boldsymbol{\eta}_i
\end{aligned}
\tag{28}
$$

Thus according to Equations (27) and (28), we have:

$$
\dot{V}_i \leq -\left|\tilde{\xi}_{1,i}\right|^{-\frac{1}{2}} \boldsymbol{\eta}_i^T \left(\boldsymbol{Q} + \Delta \boldsymbol{Q} \right) \boldsymbol{\eta}_i
\tag{29}
$$

where $\Delta \boldsymbol{Q} = - \begin{bmatrix} f_i^+ (a_i + 1) & 0 \\ 0 & f_i^+ \end{bmatrix}$ and $\boldsymbol{Q} + \Delta \boldsymbol{Q} = \dfrac{a_i}{2} \begin{bmatrix} 2b_i + a_i^2 - 2f_i^+ \frac{a_i + 1}{a_i} & -a_i \\ -a_i & 1 - \frac{2f_i^+}{a_i} \end{bmatrix}$.

From Equation (29), we can find that $\dot{V}_i$ is negative definite on condition that $\boldsymbol{Q} + \Delta \boldsymbol{Q}$ is positive definite, what is exactly the case if:

$$
\begin{cases}
a_i > 2f_i^+ \\
b_i > f_i^+ \dfrac{a_i^2}{a_i - 2f_i^+} + f_i^+ \dfrac{a_i + 1}{a_i}
\end{cases}
\tag{30}
$$

Then, analyze the finite time convergence of $\boldsymbol{\eta}_i$, according to Equation (26), we have:

$$
\left|\tilde{\xi}_{1,i}\right|^{\frac{1}{2}} < \|\boldsymbol{\eta}_i\| \leq \frac{V_i^{\frac{1}{2}}}{\lambda_{\min}^{\frac{1}{2}}(\boldsymbol{P})}
\tag{31}
$$

And according to Equations (29) and (31), we can conclude that:

$$
\begin{aligned}
\dot{V}_i \;&\leq\; -\lambda_{\min}^{\frac{1}{2}}(\boldsymbol{P}) \,\lambda_{\min}(\boldsymbol{Q} + \Delta \boldsymbol{Q}) \,\|\boldsymbol{\eta}_i\|^2 \, V_i^{-\frac{1}{2}} \\
&\leq\; -\frac{\lambda_{\min}^{\frac{1}{2}}(\boldsymbol{P}) \lambda_{\min}(\boldsymbol{Q} + \Delta \boldsymbol{Q})}{\lambda_{\max}(\boldsymbol{P})} \, V_i^{\frac{1}{2}} \\
&=\; -\gamma V_i^{\frac{1}{2}}
\end{aligned}
\tag{32}
$$

where $\gamma = \dfrac{\lambda_{\min}^{\frac{1}{2}}(\boldsymbol{P}) \lambda_{\min}(\boldsymbol{Q} + \Delta \boldsymbol{Q})}{\lambda_{\max}(\boldsymbol{P})} > 0$.

Indeed, separating variables and integrating inequality Equation (32) over the time interval $0 < \tau < t < 0$, we obtain:

$$
V_i^{\frac{1}{2}}(t) \leq -\frac{1}{2}\gamma t + V_{i,0}^{\frac{1}{2}}
\tag{33}
$$

where $V_{i,0}$ is the initial value of $V_i(t)$. Consequently, $V_i(t)$ reaches zero in a finite time T_r that is bounded by:

$$
T_r = 2V_{i,0}^{\frac{1}{2}} \gamma^{-1}
\tag{34}
$$

Therefore, accoding to [42], a STESO which is designed to satisfy Equations (21) and (30) will drive the uniformed vector of errors $\boldsymbol{\eta}_i$ and then $\tilde{\boldsymbol{\xi}}_i$ to zero in finite time T_r and will keep it at zero thereafter.

4. Design of Super Twisting Sliding Mode Controller

Sliding mode control (SMC) has been known as one of the most important tools for those systems subjected to disturbances and uncertainties, while chattering is inevitable in those methods. In order to reduce the chattering, supper twisting SMC is introduced in this section. The main objective of the FC is to guarantee that the state of attitude q and ω converge to the reference values q_d and ω_d timely. Thus, the sliding mode manifold in this article is chosen as follows:

$$s = k_1 q_e + J\omega_e \tag{35}$$

where $k_1 = \text{diag}(k_{1,x}, k_{1,y}, k_{1,z})$ is a positive defined three dimensional coefficient matrix to be designed. Take time derivative of $s = \begin{bmatrix} s_x & s_y & s_z \end{bmatrix}^T$, we have:

$$\dot{s} = k_1 \dot{q}_e + J\dot{\omega}_e \tag{36}$$

Then, submitting Equation (16) into (36):

$$\dot{s} = k_1 \dot{q}_e + u + d + J(S(\omega_e)C_d^b \omega_d - C_d^b \dot{\omega}_d) - S(\omega)J\omega \tag{37}$$

Define the control signal u as:

$$u = -\left(J(S(\omega_e)C_d^b \omega_d - C_d^b \dot{\omega}_d) - S(\omega)J\omega\right) - k_1 \dot{q}_e - k_2 \,\text{sig}\,(s)^{\frac{1}{2}} - \int_o^t k_3 \,\text{sig}\,(s)^0 d\tau - \hat{d} \tag{38}$$

and plug Equation (38) into (37), we have:

$$\dot{s} = -k_2 \,\text{sig}\,(s)^{\frac{1}{2}} - \int_o^t k_3 \,\text{sig}\,(s)^0 d\tau + \tilde{d} \tag{39}$$

where $\tilde{d} = d - \hat{d}$ is the estimation error of multiple disturbances, and according to the analysis of the previous section, $\tilde{d}$ is bounded and converges to zero in finite time. Define $\sigma = \begin{bmatrix} \sigma_x & \sigma_y & \sigma_z \end{bmatrix}^T$ as $\sigma = -\int_o^t k_3 \,\text{sig}\,(s)^0 d\tau + \tilde{d}$, then Equation (39) can be rewritten as:

$$\begin{cases} \dot{s}_i = \sigma_i - k_{2,i} \|s_i\|^{\frac{1}{2}} \,\text{sgn}\,(s_i) \\ \dot{\sigma}_i = \dot{\tilde{d}}_i - k_{3,i} \,\text{sgn}\,(s_i)\, d\tau \end{cases}, \quad i = x, y, z \tag{40}$$

where the positive defined matrix $k_2 = \text{diag}(k_{2,x}, k_{2,y}, k_{2,z})$ and $k_3 = \text{diag}(k_{3,x}, k_{3,y}, k_{3,z})$ are the controller parameters to be determined.

Subject to the restriction of article length, the convergence analysis and parameter selection rule of the STSMC will not be introduced in detail. Since Equation (40) has the same form as Equation (22), the detailed convergence analysis can refer to the contents of the previous section. Meanwhile according to Equation (30), the controller parameters can be chosen as:

$$\begin{cases} k_{2,i} > 2\left\|\dot{\tilde{d}}_i\right\| \\ k_{3,i} > \left\|\dot{\tilde{d}}_i\right\| \dfrac{k_{2,i}^2}{k_{2,i} - 2\left\|\dot{\tilde{d}}_i\right\|} + \left\|\dot{\tilde{d}}_i\right\| \dfrac{k_{2,i}+1}{k_{2,i}} \end{cases} \tag{41}$$

5. Simulation and Experimental Results

In order to evaluate the performance of the proposed control method, numerical simulation and real world experimental results are carried out in this section.

5.1. Simulation Results

We present the numerical simulations of the proposed STESO based DUEA control strategy on a model generated by the online toolbox of Quan and Dai [43], and the values of the nominal model parameters are list in Table 1.

Table 1. Quadrotor parameters used in simulation.

Parameter	Description	Value
m	Mass	1.79 kg
J_x	Roll inertia	1.335×10^{-2} kg $\cdot$ m^2
J_y	Pitch inertia	1.335×10^{-2} kg $\cdot$ m^2
J_z	Yaw inertia	2.465×10^{-2} kg $\cdot$ m^2
l	Motor moment arm	0.18 m
g	Gravity acceleration	9.81 m $\cdot$ s^{-2}
k_T	Aerodynamic coefficient	8.82×10^{-6} N/(rad/s)^2
k_D	Drag coefficient	1.09×10^{-7} N $\cdot$ m/(rad/s)^2
$\Omega_{i,max}$	Maximum rotational speed	8214 r/min
$\Omega_{i,min}$	Minimum rotational speed	100 r/min

In numerical simulations, the position of quadrotor is free and only the attitude of it is controlled. We assume that the rotor $R1$ fails in the 6th second, and loses 20% of effectiveness, which means $T_1 = 6$ s and $\alpha_1 = 0.2$ in Equation (13). Then, according to [15], the disturbance torque caused by the wind field is proportional to the wind speed, and we assume that the three-axis components of $\boldsymbol{d_w} = \begin{bmatrix} d_{w,x} & d_{w,y} & d_{w,z} \end{bmatrix}^T$ are equal $d_x = d_y = d_z = d_w$ without loss of generality. The values of $\omega_{k,i}$ are taken between 0.01π rad/s and 2.5π rad/s. The disturbance torque of wind gust used in numerical simulation is Equation (42).

$$
\begin{aligned}
d_w = \quad & 0.01 \sin\left(2.5\pi t - 3\right) + 0.02 \sin\left(2\pi t + 7\right) + 0.06 \sin\left(\pi t + 0.6\right) \\
& + 0.03 \sin\left(0.5\pi t - 9.5\right) + 0.02 \sin\left(0.3\pi t\right) + 0.12 \sin\left(0.1\pi t + 4.5\right) \\
& + 0.01 \sin\left(0.05\pi t + 2\right) + 0.003 \sin\left(0.01\pi t + 3\right) + 0.05
\end{aligned}
\tag{42}
$$

The numerical simulation is carried out in MatLab/Simulink with a fixed-sampling time of 1 ms. And to validate the performance of the proposed control strategy, two simulation cases are presented in this part. The initial conditions of the attitude angles and angular velocities are set to zero, and the desired reference commands are selected as:

$$
\Theta_{ref} = \begin{bmatrix} 15 \sin\left(0.4\pi t\right) & 15 \cos\left(0.4\pi t\right) & 0 \end{bmatrix}^T \text{ deg}
\tag{43}
$$

5.1.1. Case A: STESO vs. 2nd-Order ESO

In order to verify the enhancement of STESO relative to traditional Higher-order ESO, three comparative simulations are conducted on condition that use nonlinear PD controller as the FC. The controller gains are chosen as $\boldsymbol{K_1} = \boldsymbol{I_3}$ and $\boldsymbol{K_2} = 5\boldsymbol{I_3}$ [44], the observer gains of STESO are chosen as $a_i = 24$ and $b_i = 50$, and the bandwidth of 2nd-order ESO is chosen as 10 rad/s, i.e., the observer gains are $\boldsymbol{L} = \begin{bmatrix} 30 & 300 & 1000 \end{bmatrix}^T$ [45].

Figures 3–5 show the comparison in attitude tracking results of nonlinear PD controller with STESO, 2nd-order ESO and without DUE. From those figures, we can see that the desired attitude commands can be tracked effectively by the controller with DUE. Moreover, the tracking errors are further reduced by introducing STESO as the DUE instead of 2nd-order ESO. Figure 6 shows the comparison in lumped disturbances estimation results of STESO and 2nd-order ESO. It is obvious that compared with STESO, some phase delay exist in the estimation results of the 2nd-order ESO, which leads to its estimation error convergences into a bounded area. Meanwhile, the estimation

errors of STESO almost asymptotically convergence to zero. Especially when the disturbance torque suddenly changes, STESO has more advantages. In general, from the numerical simulation results, we can be conclude that STESO has a higher disturbance estimation accuracy, which in turn improves attitude control accuracy.
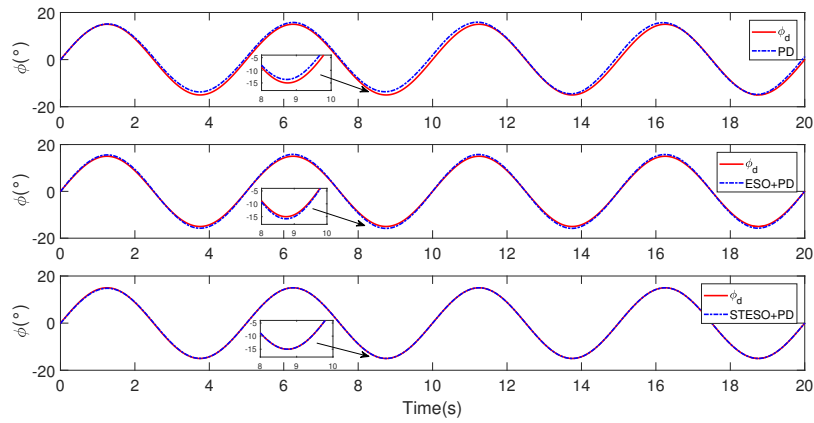

Figure 3. Simulation curves of ϕ in Case A.
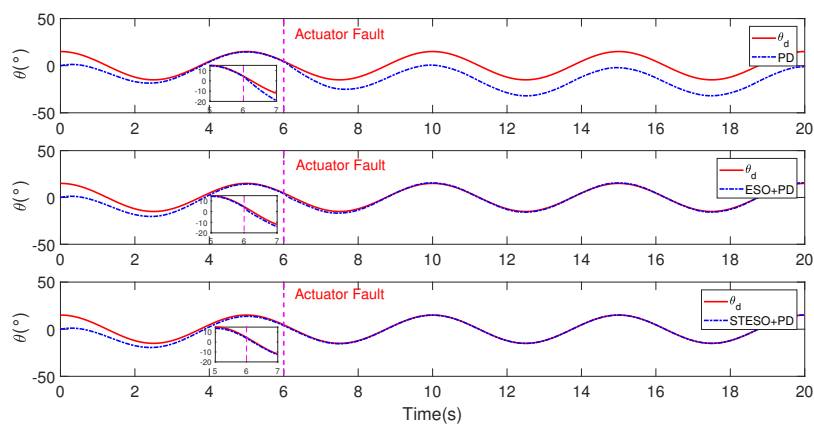

Figure 4. Simulation curves of θ in Case A.
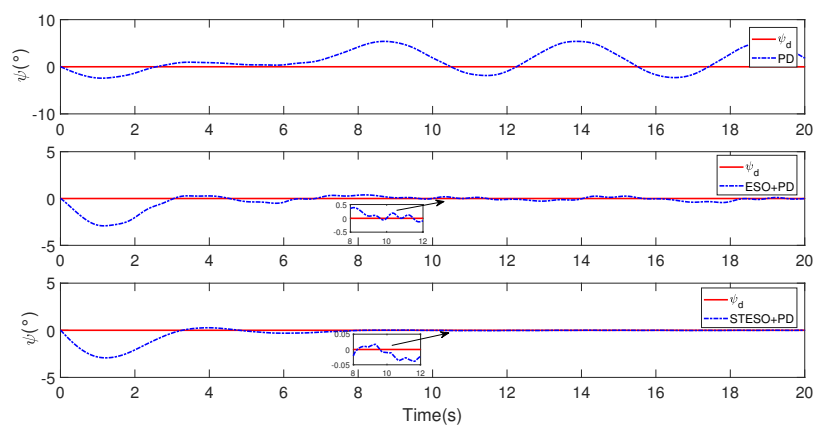
Figure 5. Simulation curves of ψ in Case A.
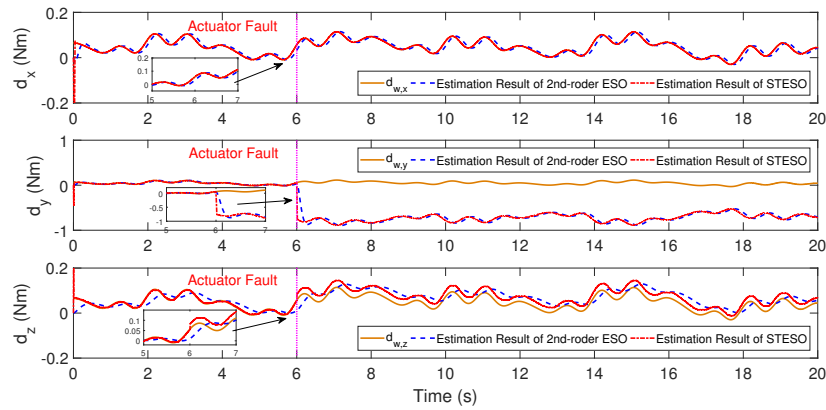
Figure 6. Disturbance estimation results in Case A.

5.1.2. Case B. STSMC vs. Nonlinear PD

In order to verify the fast convergence of STSMC, two comparative simulations are performed with the same STESO of different controllers. The controller gains of STSMC are chosen as $k_1 = \mathrm{diag}(1,1,1)$, $k_2 = \mathrm{diag}(5,5,5)$, $k_3 = \mathrm{diag}(20,20,20)$, the STESO and nonlinear PD parameters are the same with those provided in previous.

The comparison in attitude tracking results between STSMC and Nonlinear PD are illustrated in Figure 7. From this figure, we can see that quickly convergence of the attitude of quadrotor can be achieved by using STSMC as the FC. And by introducing ST algorithm into SMC, the chattering is reduced.
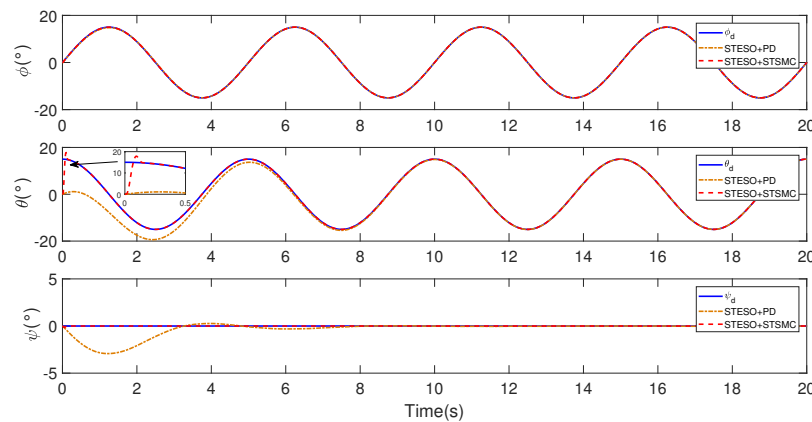
Figure 7. Simulation curves of attitude angle: STSMC vs. nonlinear PD.

5.2. Experimental Results

In order to evaluate the effectiveness of the developed algorithm in practical applications, we have also tested the proposed control scheme on a selfassembled GF360 quadrotor, where an open-source flight controller PIXHAWK [46,47] was used as the autopilot of the quadrotor.

5.2.1. Case A: STESO vs. 2nd-Order ESO

In this case, quadrotor is freely flying and we mainly aim to achieve the fast stabilization of quadrotor attitude on condition that actuator faults occur. According to the simulation results, we can conclude that STESO algorithm has advantage in quick response to the lumped disturbances. And in order to verify its effectiveness in actual flight, three comparative real time experiments are conducted to handle the sudden lose of rotor effectiveness. The experimental setup is shown in Figure 8, and freely flying is performed. As it is dangerous to damage the propeller during flight, we use software to set

up a sudden lose of rotor effectiveness in pitch channel at the 10th second. We choose the traditional nonlinear PD controller as the FC in these experiments, where the performances of the PD controller with STESO, 2nd-order ESO or without DUE are compared. The gains of the PD controller are chosen as $k_1 = \text{diag}(7, 7, 2.8)$ and $k_2 = \text{diag}(0.15, 0.15, 2)$, the gains of the STESO are $a_i = 1$ and $b_i = 0.24$, the bandwidth of the 2nd-order ESO is 4 rad/s, i.e., the observer gains are $L = \begin{bmatrix} 12 & 48 & 64 \end{bmatrix}^T$.
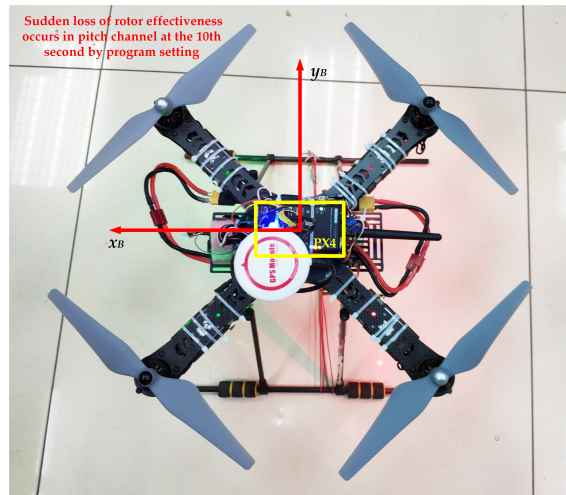
Figure 8. Experimental setup of the quadrotor hovering with sudden lose of rotor effectiveness in Case A.

The experiment curves of the attitude are plotted in Figures 9 and 10. From Figure 9, we can see that when the same loss of rotor effectiveness occurs, the deflections of pitch angle and angular rate in PD controller with STESO method are the smallest and the recovery times are the shortest. Figure 11 show the disturbances estimate curves of proposed STESO and 2nd-order ESO respectively. It can be seen that the convergence time of STESO is shorter that 2nd-order ESO. In general, the comparison of the experiment results are list detailly in Table 2. Furthermore, the corresponding control torques are shown in Figure 12.
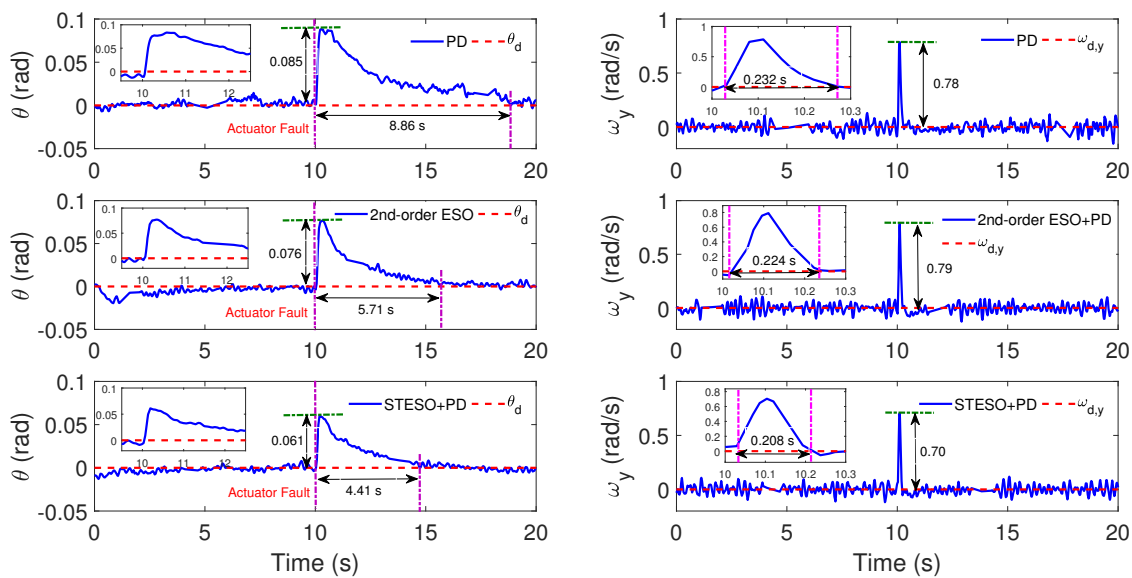

Figure 9. Experimental curves of θ and ω_y with different DUE in Case A.
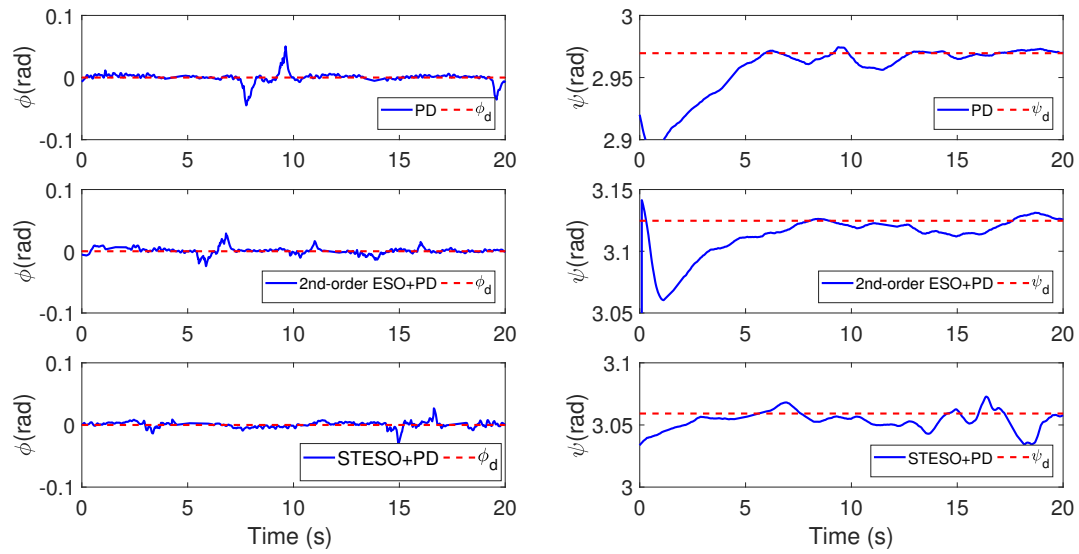
**Figure 10.** Experimental curves of ϕ and ψ with different DUE in Case A.
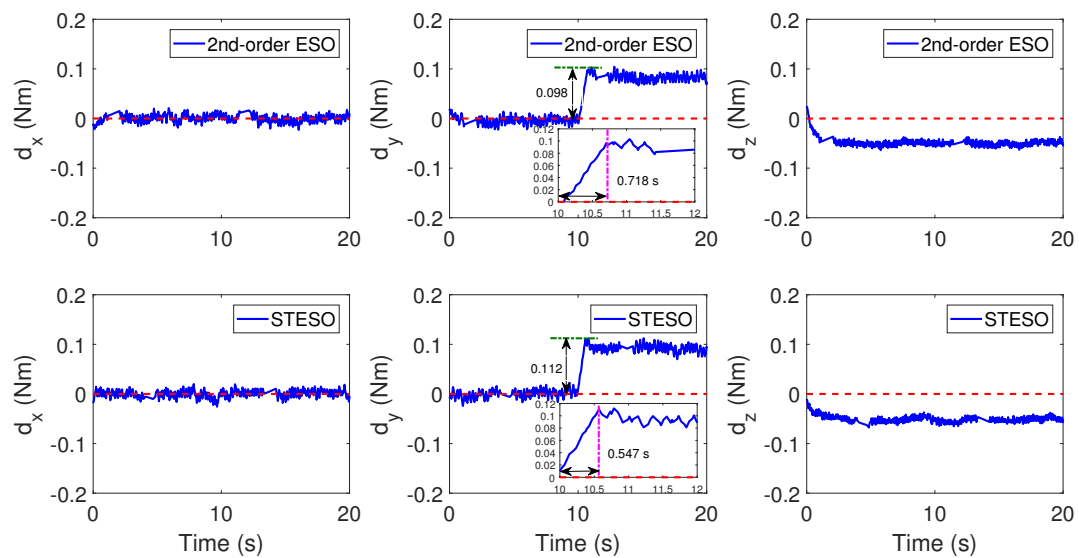
Figure 11. Disturbance estimation results of different DUE with actuator faults in Case A.

Table 2. Comparison of control performances with different observers.

	Deflection		Recovery Time		Convergence Time
	θ	ω_y	θ	ω_y	
Without Estimator	0.085 rad	0.78 rad/s	8.86 s	0.232 s	/
2nd-order ESO + PD	0.076 rad	0.79 rad/s	5.71 s	0.224 s	0.718 s
STESO + PD	0.061 rad	0.70 rad/s	4.41 s	0.208 s	0.547 s
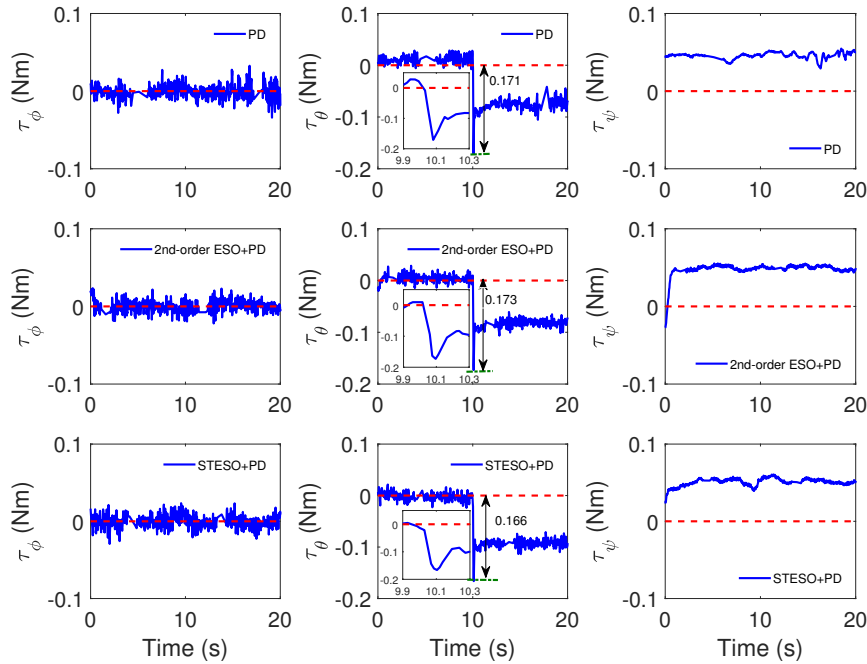
Figure 12. Control input during flight experiments in Case A.

5.2.2. Case B: Proposed Method vs. Nonlinear PD

The main propose in this case is to show the performance of the developed method for quadrotor subject to lumped disturbances such as wind disturbance and actuator fault. As shown in Figure 13, We install a damaged propeller on the $R1$ to perform the fault of the actuator, and then keep the quadrotor hovering in wind gust by remote control. In order to ensure the same experimental conditions, our experiments is run in a controlled indoor environment. We use an electrical fan with adjustable wind speed to generate the disurbance torque acting on the pitch channel of quadrotor. The average wind speed is around 4.5 m/s and turn on the electric fan at the 30 s. The experiments are carried out in our lab without GPS signals.
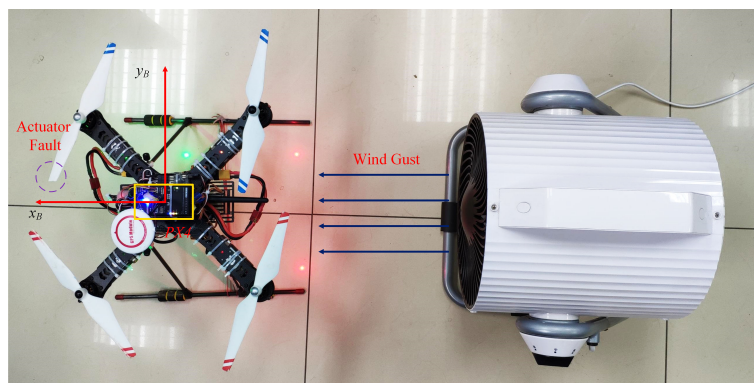
Figure 13. Experimental setup of the quadrotor hovering in the wind field in Case B.

Figure 14 shows the estimation results of the STESO. From this figure, we can see that the actuator fault in $R1$ leads to a steady disturbance torque acting on the quadrotor in hovering flight, i.e., $d_{u,x} \approx 0.04$ Nm, $d_{u,y} \approx -0.03$ Nm and $d_{u,z} \approx -0.07$ Nm. The wind gust mainly leads to the stochastic disturbance torque in each channel, plus a steady torque about -0.01 Nm in pitch channel. The attitude control results in this case are shown in Figures 15 and 16. It can be observed that the control performance is improved by introducing the proposed method compared with the nonlinear

PD controller. In addition, the root mean square (RMS) errors of the attitude angles obtained by the proposed controller and PD controller are list in Table 3. And Figure 17 illustrates the control inputs in each channel.
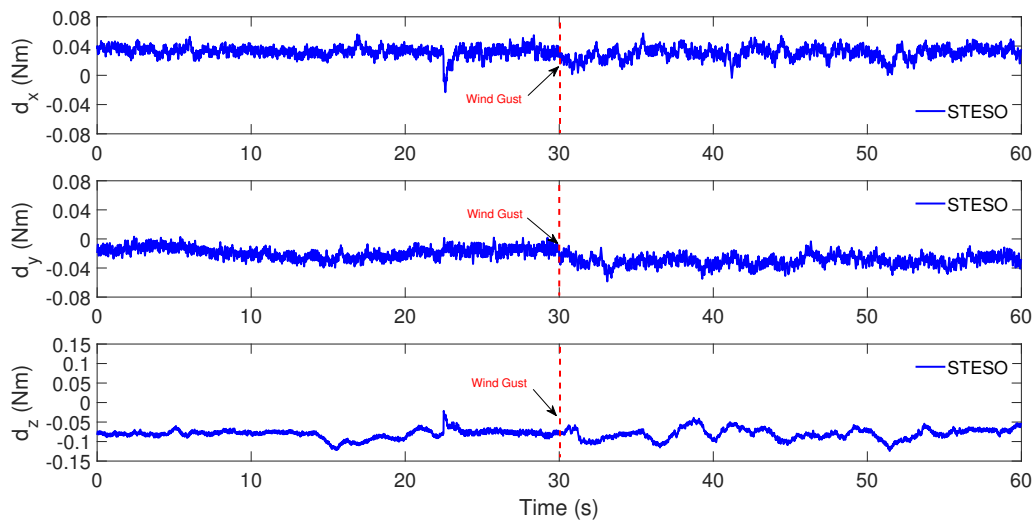

**Figure 14.** Disturbance estimation results of STESO in Case B.
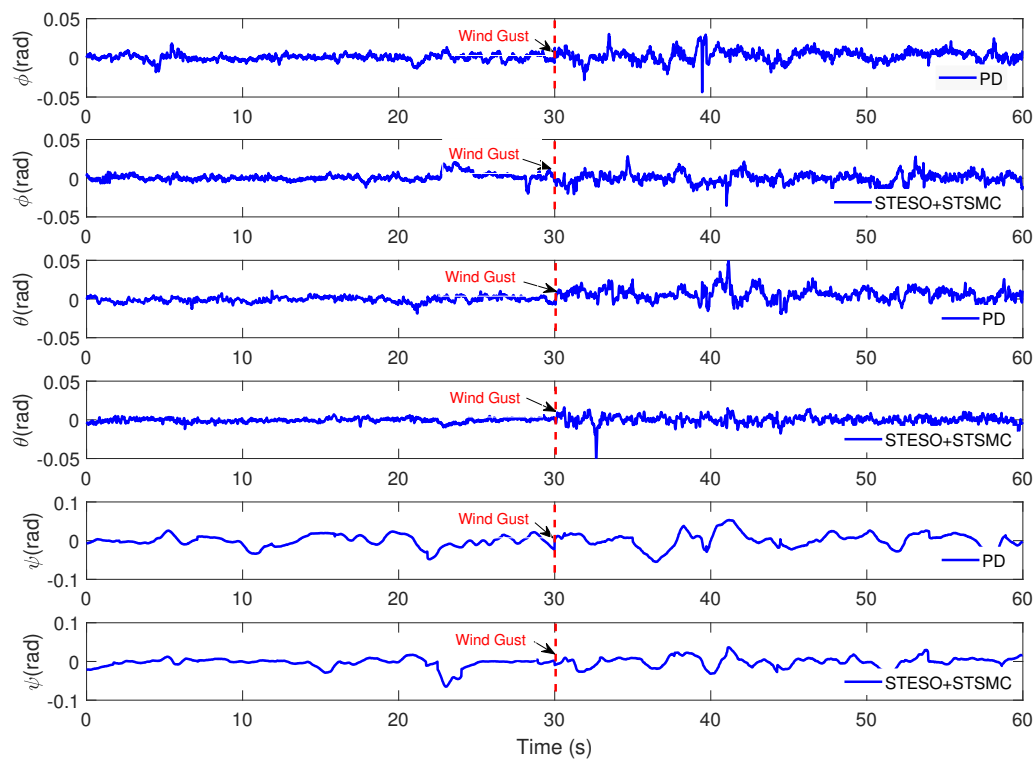
Figure 15. Experimental curves of attitude angle ϕ, θ, ψ in Case B.
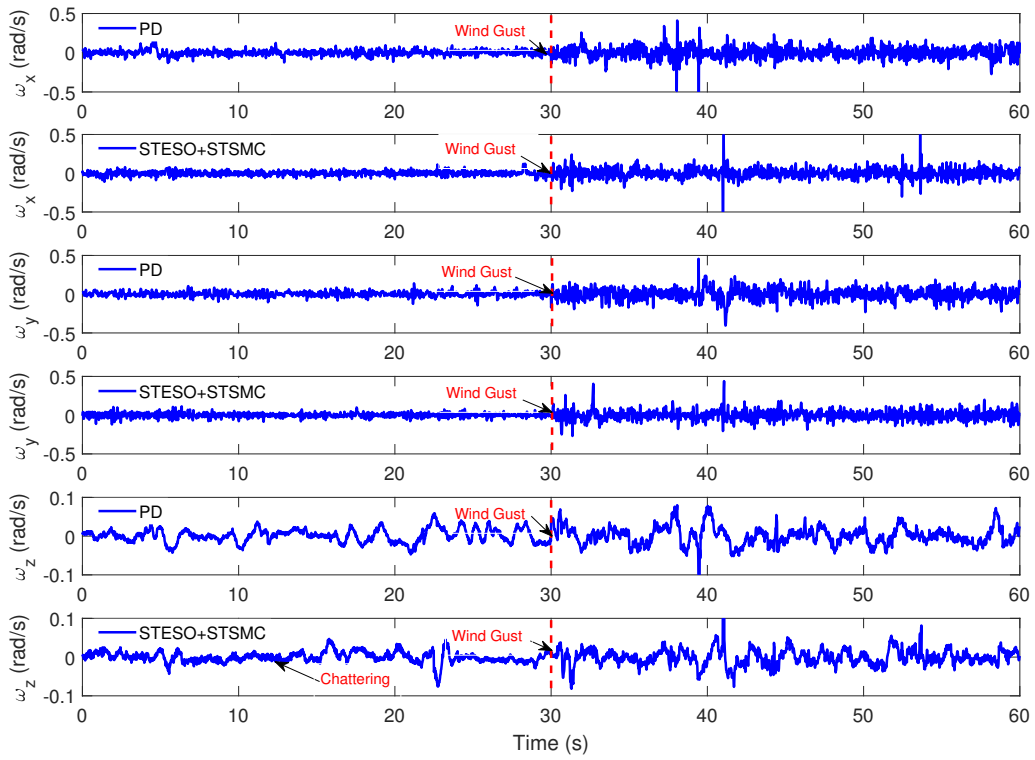
Figure 16. Experimental curves of angular rates ω_x, ω_y, ω_z in Case B.
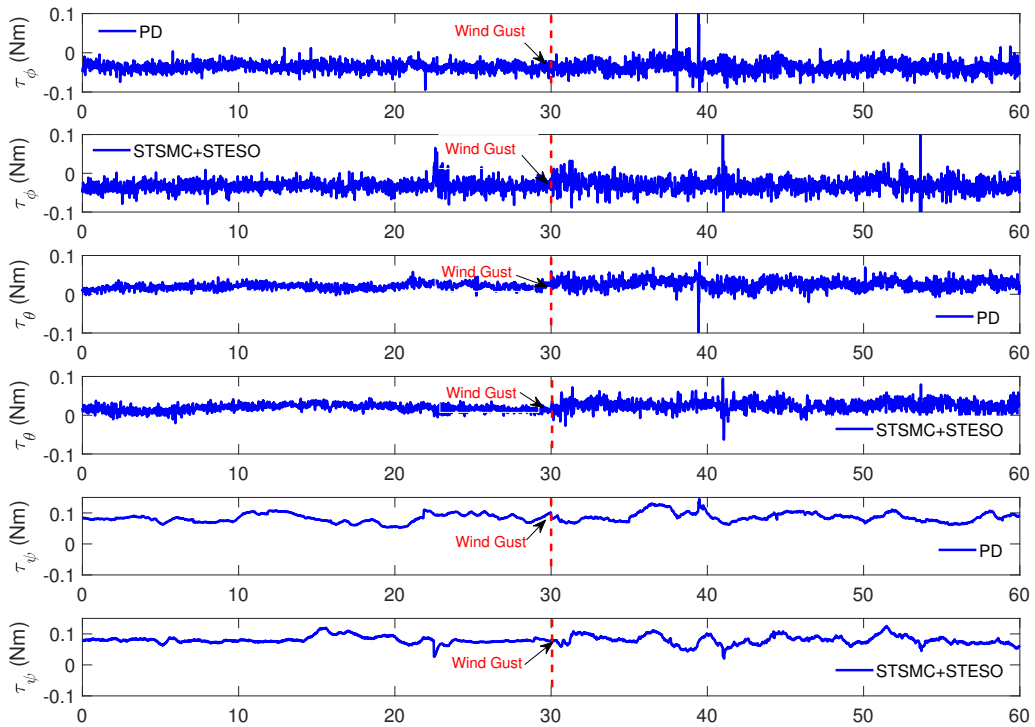
Figure 17. Control input during flight experiments in Case B.

Table 3. Comparison of attitude control performance: RMS error (rad).

	Actuator Fault Only			Actuator Fault+Wind Gust		
	ϕ	θ	ψ	ϕ	θ	ψ
nonlinear PD	0.0082	0.0072	0.0187	0.0160	0.0202	0.0204
STESO + STSMC	0.0094	0.0052	0.0135	0.0136	0.0116	0.0132

6. Conclusions

In this paper, the problem of high precision attitude tracking for quadrotor in the presence of wind gust and actuator fault is investigated. In order to estimate and attenuate the disturbances timely and accurately, a STESO is proposed and successfully implemented as the DUE in experiments. Also, a STSMC is designed as the FC to drive the attitude angle and angular velocity to their desired value in finite time. From the comparative simulation and experiment results, we can conclude that when the parameter selection rule given in this article of is satisfied, the proposed super-twisting algorithm based controller can relize the fast converge to the desired attitude precisely with less chattering. And compared with the traditional Higher-order ESO, STESO has a higher disturbance estimation accuracy, which in turn improves attitude control accuracy.

References

1. Stepaniak, M.J.; van Graas, F.; de Haag, M.U. Design of an Electric Propulsion System for a Quadrotor Unmanned Aerial Vehicle. *J. Aircr.* **2009**, *46*, 1050–1058. [CrossRef]
2. Gupte, S.; Mohandas, P.I.T.; Conrad, J.M. A Survey of Quadrotor Unmanned Aerial Vehicles. In Proceedings of the IEEE Southeastcon, Orlando, FL, USA, 15–18 March 2012 .
3. Ozbek, N.S.; Onkol, M.; Efe, M.O. Feedback control strategies for quadrotor-type aerial robots: A survey. *Trans. Inst. Meas. Control* **2016**, *38*, 529–554. [CrossRef]
4. Bouabdallah, S.; Becker, M.; Siegwart, R. Autonomous miniature flying robots: Coming soon! *IEEE Robot Autom Mag.* **2007**, *14*, 88–98. [CrossRef]
5. Han, W.X.; Wang, Z.H.; Shen, Y. Fault estimation for a quadrotor unmanned aerial vehicle by integrating the parity space approach with recursive least squares. *Proc. Inst. Mech. Eng. Part G J. Aerosp. Eng.* **2018**, *232*, 783–796. [CrossRef]
6. Tian, B.L.; Ma, Y.X.; Zong, Q. A Continuous Finite-Time Output Feedback Control Scheme and Its Application in Quadrotor UAVs. *IEEE Access* **2018**, *6*, 19807–19813. [CrossRef]
7. Huang, M.; Xian, B.; Diao, C.; Yang, K.Y.; Feng, Y. Adaptive Tracking Control of Underactuated Quadrotor Unmanned Aerial Vehicles via Backstepping. In Proceedings of the 2010 American Control Conference, Baltimore, MD, USA, 30 June–2 July 2010; pp. 2076–2081.
8. Salih, A.L.; Moghavvemi, M.; Mohamed, H.A.F.; Gaeid, K.S. Flight PID controller design for a UAV quadrotor. *Sci. Res. Essays* **2010**, *5*, 3660–3667.
9. Lee, K.U.; Kim, H.S.; Park, J.B.; Choi, Y.H. Hovering Control of a Quadrotor. In Proceedings of the 2012 12th International Conference on Control, Automation and Systems (Iccas), JeJu Island, Korea, 17–21 October 2012; pp. 162–167.
10. González-Vázquez, S.; Moreno-Valenzuela, J. A New Nonlinear PI/PID Controller for Quadrotor Posture Regulation. In Proceedings of the 2010 IEEE Electronics, Robotics and Automotive Mechanics Conference, Morelos, Mexico, 28 September–1 October 2010; pp. 642–647.

11. González-Vázquez, S.; Moreno-Valenzuela, J. Motion Control of a Quadrotor Aircraft via Singular Perturbations. *Int. J. Adv. Robot. Syst.* **2013**, *10*, 368. [CrossRef]

12. Liu, H.; Lu, G.; Zhong, Y.S. Robust LQR Attitude Control of a 3-DOF Laboratory Helicopter for Aggressive Maneuvers. *IEEE Trans. Ind. Electron.* **2013**, *60*, 4627–4636. [CrossRef]

13. Munoz, F.; Gonzalez-Hernandez, I.; Salazar, S.; Espinoza, E.S.; Lozano, R. Second order sliding mode controllers for altitude control of a quadrotor UAS: Real-time implementation in outdoor environments. *Neurocomputing* **2017**, *233*, 61–71. [CrossRef]

14. Avram, R.C.; Zhang, X.D.; Muse, J. Nonlinear Adaptive Fault-Tolerant Quadrotor Altitude and Attitude Tracking With Multiple Actuator Faults. *IEEE Trans. Control Syst. Technol.* **2018**, *26*, 701–707. [CrossRef]

15. Wang, C.; Song, B.F.; Huang, P.F.; Tang, C.H. Trajectory Tracking Control for Quadrotor Robot Subject to Payload Variation and Wind Gust Disturbance. *J. Intell. Robot. Syst.* **2016**, *83*, 315–333. [CrossRef]

16. Basri, M.A.M.; Husain, A.R.; Danapalasingam, K.A. Stabilization and trajectory tracking control for underactuated quadrotor helicopter subject to wind-gust disturbance. *Sadhana Acad. Proc. Eng. Sci.* **2015**, *40*, 1531–1553. [CrossRef]

17. Chen, W.H.; Ohnishi, K.; Guo, L. Advances in Disturbance/Uncertainty Estimation and Attenuation. *IEEE Trans. Ind. Electron.* **2015**, *62*, 5758–5762. [CrossRef]

18. Yang, J.; Chen, W.H.; Li, S.H.; Guo, L.; Yan, Y.D. Disturbance/Uncertainty Estimation and Attenuation Techniques in PMSM Drives-A Survey. *IEEE Trans. Ind. Electron.* **2017**, *64*, 3273–3285. [CrossRef]

19. Wang, Z.; Wu, Z. Nonlinear attitude control scheme with disturbance observer for flexible spacecrafts. *Nonlinear Dyn.* **2015**, *81*, 257–264. [CrossRef]

20. Wang, Z.; Wu, Z.; Du, Y.J. Adaptive sliding mode backstepping control for entry reusable launch vehicles based on nonlinear disturbance observer. *Proc. Inst. Mech. Eng. Part G J. Aerosp. Eng.* **2016**, *230*, 19–29. [CrossRef]

21. Pu, Z.Q.; Yuan, R.Y.; Yi, J.Q.; Tan, X.M. A Class of Adaptive Extended State Observers for Nonlinear Disturbed Systems. *IEEE Trans. Ind. Electron.* **2015**, *62*, 5858–5869. [CrossRef]

22. Wang, H.D.; Huang, Y.B.; Xu, C. ADRC Methodology for a Quadrotor UAV Transporting Hanged Payload. In Proceedings of the 2016 IEEE International Conference on Information and Automation (ICIA), Ningbo, China, 1–3 August 2016; pp. 1641–1646.

23. Xia, Y.Q.; Pu, F.; Li, S.F.; Gao, Y. Lateral Path Tracking Control of Autonomous Land Vehicle Based on ADRC and Differential Flatness. *IEEE Trans. Ind. Electron.* **2016**, *63*, 3091–3099. [CrossRef]

24. Dou, J.X.; Kong, X.X.; Wen, B.C. Altitude and attitude active disturbance rejection controller design of a quadrotor unmanned aerial vehicle. *Proc. Inst. Mech. Eng. Part G J. Aerosp. Eng.* **2017**, *231*, 1732–1745. [CrossRef]

25. Busawon, K.K.; Kabore, P. Disturbance attenuation using proportional integral observers. *Int. J. Control* **2001**, *74*, 618–627. [CrossRef]

26. Gao, Z.W.; Breikin, T.; Nang, H. Discrete-time proportional and integral observer and observer-based controller for systems with both unknown input and output disturbances. *Opt. Control Appl. Meth.* **2008**, *29*, 171–189. [CrossRef]

27. Alcan, G.; Unel, M. Robust Hovering Control of a Quadrotor Using Acceleration Feedback. In Proceedings of the 2017 International Conference on Unmanned Aircraft Systems (Icuas'17), Miami, FL, USA, 13–16 June 2017; pp. 1455–1462.

28. Han, J.Q. From PID to Active Disturbance Rejection Control. *IEEE Trans. Ind. Electron.* **2009**, *56*, 900–906. [CrossRef]

29. Wang, W.; Gao, Z. A comparison study of advanced state observer design techniques. In Proceedings of the American Control Conference, Denver, CO, USA, 4–6 June 2003; Volume 6, pp. 4754–4759

30. Madonski, R.; Herman, P. Survey on methods of increasing the efficiency of extended state disturbance observers. *ISA Trans.* **2015**, *56*, 18–27. [CrossRef] [PubMed]

31. Godbole, A.A.; Kolhe, J.P.; Talole, S.E. Performance Analysis of Generalized Extended State Observer in Tackling Sinusoidal Disturbances. *IEEE Trans. Control Syst. Technol.* **2013**, *21*, 2212–2223. [CrossRef]

32. Madani, T.; Benallegue, A. Sliding mode observer and backstepping control for a quadrotor unmanned aerial vehicles. In Proceedings of the 2007 American Control Conference, New York, NY, USA, 9–13 July 2007; Volume 1–13, pp. 2462–2467.

33. Chuei, R.; Cao, Z.W.; Man, Z.H. Super Twisting Observer based Repetitive Control for Aperiodic Disturbance Rejection in a Brushless DC Servo Motor. *Int. J. Control Autom. Syst.* **2017**, *15*, 2063–2071. [CrossRef]

34. Utkin, V. On Convergence Time and Disturbance Rejection of Super-Twisting Control. *IEEE Trans. Autom. Control* **2013**, *58*, 2013–2017. [CrossRef]

35. Li, P.; Ma, J.J.; Zheng, Z.Q. Disturbance-observer-based fixed-time second-order sliding mode control of an air-breathing hypersonic vehicle with actuator faults. *Proc. Inst. Mech. Eng. Part G J. Aerosp. Eng.* **2018**, *232*, 344–361. [CrossRef]

36. Tian, B.L.; Liu, L.H.; Lu, H.C.; Zuo, Z.Y.; Zong, Q.; Zhang, Y.P. Multivariable Finite Time Attitude Control for Quadrotor UAV: Theory and Experimentation. *IEEE Trans. Ind. Electron.* **2018**, *65*, 2567–2577. [CrossRef]

37. Chovancova, A.; Fico, T.; Hubinsky, P.; Duchon, F. Comparison of various quaternion-based control methods applied to quadrotor with disturbance observer and position estimator. *Robot. Auton. Syst.* **2016**, *79*, 87–98. [CrossRef]

38. Bouabdallah, S.; Siegwart, R. Full control of a quadrotor. In Proceedings of the 2007 IEEE/RSJ International Conference on Intelligent Robots and Systems, San Diego, CA, USA, 29 October–2 November 2007; Volume 9, pp. 153–158.

39. Waslander, S.; Wang, C. Wind Disturbance Estimation and Rejection for Quadrotor Position Control. In Proceedings of the AIAA Infotech@Aerospace Conference and AIAA Unmanned...Unlimited Conference, Seattle, WA, USA, 6–9 April 2009.

40. Chen, Y.M.; He, Y.L.; Zhou, M.F. Decentralized PID neural network control for a quadrotor helicopter subjected to wind disturbance. *J. Cent. South Univ.* **2015**, *22*, 168–179. [CrossRef]

41. Önder, E.M. Battery power loss compensated fractional order sliding mode control of a quadrotor UAV. *Asian J. Control 14*, 413–425.

42. Shtessel, Y.; Edwards, C.; Fridman, L.; Levant, A. *Sliding Mode Control and Observation*; Springer: New York, NY, USA, 2014.

43. Quan, Q.; Dai, X. Flight Performance Evaluation of UAVs. Available online: http://flyeval.com/ (accessed on 20 April 2018).

44. Shi, D.; Wu, Z.; Chou, W. Harmonic Extended State Observer Based Anti-Swing Attitude Control for Quadrotor with Slung Load. *Electronics* **2018**, *7*, 83. [CrossRef]

45. Shi, D.; Wu, Z.; Chou, W. Generalized Extended State Observer Based High Precision Attitude Control of Quadrotor Vehicles Subject to Wind Disturbance. *IEEE Access* **2018**, *6*, 2169–3536. [CrossRef]

46. Meier, L.; Tanskanen, P.; Heng, L.; Lee, G.H.; Fraundorfer, F.; Pollefeys, M. PIXHAWK: A micro aerial vehicle design for autonomous flight using onboard computer vision. *Auton. Robot.* **2012**, *33*, 21–39. [CrossRef]

47. Meier, L.; Tanskanen, P.; Fraundorfer, F.; Pollefeys, M. The Pixhawk Open-Source Computer Vision Framework for Mavs. In Proceedings of the International Conference on Unmanned Aerial Vehicle in Geomatics (UAV-G), New York, NY, USA, 14–16 September 2011; Volume 38-1, pp. 13–18.